To be Presented at III International
Round Table Meeting On Sintering,
September 3-8, 1973, Herceg Novi,
Yugoslavia

LBL-1495
c.1

THERMODYNAMICS OF SOLID STATE SINTERING

Carl E. Hoge and Joseph A. Pask

March 1973

Prepared for the U.S. Atomic Energy
Commission under Contract W-7405-ENG-48

For Reference

Not to be taken from this room

LBL-1495
c.1

DISCLAIMER

This document was prepared as an account of work sponsored by the United States Government. While this document is believed to contain correct information, neither the United States Government nor any agency thereof, nor the Regents of the University of California, nor any of their employees, makes any warranty, express or implied, or assumes any legal responsibility for the accuracy, completeness, or usefulness of any information, apparatus, product, or process disclosed, or represents that its use would not infringe privately owned rights. Reference herein to any specific commercial product, process, or service by its trade name, trademark, manufacturer, or otherwise, does not necessarily constitute or imply its endorsement, recommendation, or favoring by the United States Government or any agency thereof, or the Regents of the University of California. The views and opinions of authors expressed herein do not necessarily state or reflect those of the United States Government or any agency thereof or the Regents of the University of California.

0 0 0 0 3 9 0 0 3 7 3

THERMODYNAMICS OF SOLID STATE SINTERING

Carl E. Hoge and Joseph A. Pask*

Inorganic Materials Research Divison, Lawrence Berkeley Laboratory
and Department of Materials Science and Engineering,
College of Engineering; University of California,
Berkeley, California 94720

ABSTRACT

A thermodynamic analysis of solid state sintering of a single phase isotropic material of uniform particle size indicates that the ratio of the solid/solid and solid/vapor interfacial energies (γ_{ss}/γ_{sv}) is critical; in order to realize theoretical density it must be smaller for less dense packings of unfired compacts. Another critical requirement is that pores must remain on grain boundaries during sintering. Pores on planar grain boundaries are effectively pinned. Curved grain boundaries can break away from pores when they achieve critical curvatures; this feature is essentially independent of γ_{ss}/γ_{sv} or the corresponding dihedral angle in the normal range of values. Non-uniform particle or grain size distribution thus must be avoided since they lead to grain boundary curvatures.

---

*Graduate research assistant and professor of ceramic engineering, respectively.

This work was done under the auspices of the United States Atomic Energy Commission.

Introduction

The basic driving force for the sintering of a particulate compact of equilibrium composition is the reduction in free energy of the compact which arises through the reduction in the surface (solid/vapor interface) area of the compact. Also, in cases where theoretical density is desired, pores must be associated with grain boundaries (solid/solid interfaces) during the entire sintering process; i.e., isolated pores should not develop. Thermodynamic analyses identify the conditions under which these objectives can be realized.

Thermodynamics of End-Point Densities

As the solid/vapor interfacial area decreases, the solid/solid interfacial area increases. The change in free energy of the system at constant temperature, pressure and mole fraction can then be expressed as

$$\delta(G_{syst}) = \delta \int \gamma_{sv} dA_{sv} + \delta \int \delta_{ss}\, dA_{ss} \qquad (1)$$

where

γ_{sv} = solid/vapor interfacial energy

γ_{ss} = solid/solid interfacial energy

dA_{sv} = differential solid/vapor interfacial area

dA_{ss} = differential solid/solid interfacial area

As long as $\delta(G)$ remains equal to or less than zero, sintering will continue. The first term on the right of the equation is always negative and the second, positive. Therefore, $\delta(G)$ will be a function of the relative interfacial areas (geometry of the system) and interfacial energies.

Three sintering geometries were analyzed for spherical particles of uniform size: simple cubic, body-centered cubic, and face-centered cubic packing. The particles are assumed to be crystalline, and their interfacial energies to be isotropic. The interfacial energies are related as:

$$\gamma_{ss} = 2\gamma_{sv} \cos \phi/2 \qquad (2)$$

where ϕ is the dihedral angle.

The analysis for simple cubic packing is as follows. Figure 1A shows a simple cubic cell with eight particles at the corners of a cube, corresponding to one particle with a coordination of six per unit cell. Figure 1B shows the mass distribution on densification at a contact or grain boundary between two spheres. As the cap material is removed, the particle centers move together and the radii of the spheres increase, keeping the total volume constant. Then, from Fig. 1B, for a particle in a unit cell with six contacts

$$A_{sv} = 4\pi R^2 - 6(2\pi Rh) \qquad (3)$$

where R is the radius of the sphere at any degree of densification and h is the height of the spherical segment. Setting P as a variable equal to h/R (similar to White and Stevenson[1])

$$\frac{A_{sv}}{\pi} = 4R^2(1-3P) \qquad (4)$$

The original particle radius, R_o, and R are related by

$$R^3 = \frac{4R_o^3}{4-18P^2 + 6P^3} \tag{5}$$

By substituting (5) into (4)

$$\frac{A_{sv}}{\pi R_o^2} = \frac{4(4)^{2/3}(1-3P)}{(4-18P^2 + 6P^3)^{2/3}} \tag{6}$$

and on differentiating

$$d\left(\frac{A_{sv}}{\pi R_o^2}\right) = \frac{24(4)^{2/3}(-2 -5P^2 + 4P + 3P^3)}{(4-18P^2 + 6P^3)^{5/3}} \tag{7}$$

Since each solid/solid contact is shared by two spheres, the solid/solid area per unit cell sphere is expressed as

$$\frac{A_{ss}}{\pi} = \frac{6(2Rh-h^2)}{2} \tag{8}$$

where $\frac{2Rh-h^2}{2}$ is half the boundary area per contact for a single sphere. By substituting (5) into (8) and PR for h

$$\frac{A_{ss}}{\pi R_o^2} = \frac{3(4)^{2/3}(2P-P^2)}{(4-18P^2 + 6P^3)^{2/3}} \tag{9}$$

and on differentiating,

$$\frac{dA_{ss}}{\pi R_o^2} = 12(4)^{2/3}(2 + 3P^2-2P)/(4-18P^2 + 6P^3)^{5/3} \tag{10}$$

Substituting (10) and (7) into (1)

$$\delta(G_{syst}) = \pi R_o^2\ \gamma_{sv}(24)(4)^{2/3}(-2-5P^2 + 4P + 3P^3)/(4-18P^2 + 6P^5)^{5/3}$$

$$+ \pi R_o^2\ \gamma_{ss}(12)(4)^{2/3}(2 + 3P^2-2P)/(4-15P^2 + 6P^5)^{5/3} \tag{11}$$

and setting $\delta(G_{syst}) = 0$

$$\frac{\gamma_{ss}}{\gamma_{sv}} = \frac{-2(-2-5P^2 + 4P + 3P^3)}{(2 + 3P^2 -2P)} \tag{12}$$

A similar procedure was used for the other packing arrangements. The results for the body-centered cubic packing of particles (with a coordination number of eight) was found to be

$$\frac{\gamma_{ss}}{\gamma_{sv}} = \frac{-2(-1-3P^2 + 2P^3 + 2P)}{(1 + 2P^3-P)} \tag{13}$$

and for face-centered cubic packing (with a coordination number of twelve),

$$\frac{\gamma_{ss}}{\gamma_{sv}} = \frac{-2(-1-4P^2 + 3P^3 + 2P)}{(1 + 3P^2-P)} \tag{14}$$

Equations (12), (13), and (14) determine the ratio of γ_{ss}/γ_{sv} as a function of densification for which $\delta(G_{syst}) = 0$.

The fractional starting void volume for simple cubic packing of spheres is 0.48; for body-centered cubic, 0.32; and for face-centered cubic, 0.26. As densification or sintering proceeds h/R, or P, increases. Then, by equating the void volume with the material removed from the spherical caps as a function of P, densification was found to be complete at P = 0.347, P = 0.205, and P = 0.110, respectively, for the three types of packings.

Figure 2 is a plot of h/R, or P, versus γ_{ss}/γ_{sv} for (12), (13), and (14); the plots lie on the same straight line. Critical ratios of γ_{ss}/γ_{sv} for which complete densification can be obtained are determined by the above critical values of P. Therefore, as shown in the figure, for simple cubic packing the critical value for γ_{ss}/γ_{sv} is 1.31; for body-centered cubic, 1.58; and for face-centered cubic, 1.78. Since this ratio is directly related to the dihedral angle as shown in (2), the corresponding critical values for ϕ are 98°, 74°, and 53°, respectively.

For a particular packing arrangement, any ratio of γ_{ss}/γ_{sv} less, or any value of ϕ greater, than the critical value can lead to complete or theoretical densification. In real systems where packing is not uniform the critical values will probably be determined by the coordination number of the particles in the less dense regions.

Starting with (1) and using (3), (8) and the critical ratio of γ_{ss}/γ_{sv} for simple cubic packing, a plot of the net integral normalized free energy change vs h/R can be made as shown in Fig. 3. The graph also shows the integral free energy changes due to the solid/vapor and

solid/solid area changes. It can be seen that ΔG decreases as h/R, or P, increases and reaches a minimum at the critical value of P of 0.347 where $\delta(G_s)$ is zero. Higher values of P are unrealistic since the system is already dense at this point. Similar analyses were obtained for compacts with body-centered cubic and face-centered cubic packings.

The dihedral angle under equilibrium conditions is important in that it reveals the γ_{ss}/γ_{sv} ratio for a given system. In many cases of solid state sintering ϕ is greater than 120° due to the fact that γ_{ss} is less than γ_{sv}. The present analysis indicates that theoretical density should be achieved in these cases. Lack of complete densification then must be due to other factors such as movement of grain boundaries past pores leaving them isolated, entrapment of gases, or poor processing resulting in extreme non-uniformity of packing and/or aggregation.

On the other hand, a system that does not densify and whose dihedral angle is less than 98°, which is the critical angle for simple cubic packing, can realize densification in two ways. The density of the unfired compact can be increased assuming that the packing is uniform throughout the compact; this procedure would lower the critical angle for complete densification. Secondly, the dihedral angle may be altered by the addition of impurities that segregate at interfaces thus altering γ_{ss} and γ_{sv} resulting in a reduced γ_{ss}/γ_{sv} ratio.

In any case, the pores must remain associated with grain boundaries throughout the entire densification process until they are gone.

Thermodynamics of Grain Growth

It has long been realized that if the pores stay at the grain boundaries during sintering, they have a much better chance of being annihalated than if they are trapped as isolated spherical pores at large diffusion distances from grain boundaries.[2,3,4] The fact that isolated pores lead to densities less than theoretical while pores which remain at grain boundaries lead to theoretical density is well known. It has been argued that in order to achieve theoretical density, the grain boundaries must be prohibited from sweeping out past pores thus leaving them isolated. Therefore, in numerous sintering studies, additives are introduced to compacts for the stated purpose of pinning grain boundaries. In some cases, the additive acts as a sparingly soluble second phase which segregates at grain boundaries; the analysis is then modified from that being discussed in this report.

A. Lenticular Pore at a Planar Grain Boundary

It is of interest to examine the thermodynamics of a planar grain boundary breaking away from a lenticular shaped pore. The geometry to be examined in detail is shown in Fig. 4; the isolated pore becomes spherical as the grain boundary moves away. This process increases the free energy of the system because solid/solid interfacial area is created but also reduces the free energy because solid/vapor interfacial area is reduced due to the pore shape change. Therefore, the net free energy of the system will be a function of the relative interfacial areas and energies. The analysis proceeds as follows.

From Fig. 4, half the dihedral angle is given by

$$\cos \phi/2 = \frac{r^2-h^2}{r^2+h^2} \tag{15}$$

where r is the radius of the lenticular pore. From (2) and by setting $\gamma_{ss}/2\gamma_{sv}$ equal to A, we get

$$A = \frac{r^2-h^2}{r^2+h^2} \tag{16}$$

Algebraic manipulation leads to

$$h^2 = \frac{r^2(1-A)}{(1+A)} \tag{17a}$$

$$h = \frac{r(1-A)^{1/2}}{(1+A)^{1/2}} \tag{17b}$$

Referring to Fig. 4, the change in free energy of the system is

$$\Delta G_{syst} = G_{II} - G_I \tag{18}$$

where $G_{II} = A_{ss}^{II}\,\gamma_{ss} + A_{sv}^{II}\,\gamma_{sv}$,

and $G_I = A_{ss}^{I}\,\gamma_{ss} + A_{sv}^{I}\,\gamma_{sv}$

Therefore,

$$\Delta G_{syst} = \gamma_{ss}(A_{ss}^{II} - A_{ss}^{I}) + \gamma_{sv}(A_{sv}^{II} - A_{sv}^{I}) \tag{19a}$$

$$\Delta G_{syst} = \gamma_{ss}\ \Delta A_{ss} + \gamma_{sv}\ \Delta A_{sv} \tag{19b}$$

If we consider the overall area of the grain boundary to be fixed and circular, then

$$A_{ss}^{II} = \pi(\ell-r)^2-\pi r^2 \tag{20}$$

and

$$A_{ss}^{II} = \pi(\ell-r)^2 \tag{21}$$

where ℓ is the radius of the planar grain boundary. Thus

$$\Delta A_{ss} = \pi(\ell-r)^2-\pi(\ell-r)^2 + \pi r^2 \tag{22a}$$

$$\Delta A_{ss} = \pi r^2 \tag{22b}$$

The solid-vapor area of the lenticular pore is given by

$$A_{sv}^{I} = 2(2\pi Rh) \tag{23}$$

If we substitute

$$R = \frac{r^2 + h^2}{2h}$$

obtained from geometry (Fig. 4) into (23), then

$$A_{sv}^{I} = \frac{2(2\pi h)(r^2 + h^2)}{2h} \tag{24a}$$

$$A_{sv}^{I} = \pi 2(r^2 + h^2) \tag{24b}$$

When the grain boundary moves, the volume of the resulting pore remains constant. The volume of the lenticular pore is

$$V_{sv}^{I} = 2\left(\frac{\pi}{6}\ h(3r^2 + h^2)\right) \tag{25}$$

and the volume of the spherical pore is

$$V_{sv}^{II} = \frac{4\pi q^3}{3} \tag{26}$$

where q is the radius of the spherical pore. Equating (25) and (26) results in

$$q^2 = \left[\frac{h(3r^2 + h^2)}{4}\right]^{2/3} \tag{27}$$

Substituting this value for q^2 into

$$A_{sv}^{II} = 4\pi q^2 \tag{28}$$

gives the value of the resulting spherical pore in terms of r and h

$$A_{sv}^{II} = \frac{4\pi}{4^{2/3}} \left[h(3r^2 + h^2) \right]^{2/3} \tag{29a}$$

$$A_{sv}^{II} = 4^{1/3}\ \pi(h(3r^2 + h^2))^{2/3} \tag{29b}$$

Then, combining (24b) and (29b)

$$\Delta A_{sv} = 4^{1/3}\ \pi(h(3r^2 + h^2))^{2/3} - 2\pi(r^2 + h^2) \tag{30}$$

Substituting (22b) and (30) into (19b), we get

$$\Delta G_{syst} = \gamma_{ss}\pi r^2 + \gamma_{sv} \left\{ 4^{1/3}\ \pi(h(3r^2 + h^2))^{2/3} - 2\pi(r^2 + h^2) \right\} \tag{31a}$$

$$\frac{\Delta G_{syst}}{\pi} = \gamma_{ss} r^2 + \gamma_{sv} \left\{ 4^{1/3}\ (h(3r^2 + h^2))^{2/3} - 2(r^2 + h^2) \right\}. \tag{31b}$$

Further substitution of (17) into (31b) gives

$$\frac{\Delta G_{syst}}{\pi} = \gamma_{ss} r^2 + \gamma_{sv} \left\{ 4^{1/3} \left[\left(\frac{1-A}{1+A} \right)^{1/2} r \left(3r^2 + r^2 \left(\frac{1-A}{1+A} \right) \right) \right]^{2/3} \right.$$

$$\left. -2\left(r^2 + r^2 \left(\frac{1-A}{1+A} \right) \right) \right\} \tag{32a}$$

$$\frac{\Delta G_{syst}}{\pi} = \gamma_{ss} r^2 + \gamma_{sv} r^2 \left\{ 4^{1/3} \left[\left(\frac{1-A}{1+A} \right)^{1/2} \left(\frac{4+2A}{1+A} \right) \right]^{2/3} - \frac{4}{1+A} \right\} \tag{32b}$$

Then, substituting $2A\gamma_{sv}$ for γ_{ss} we get

$$\frac{\Delta G_{syst}}{\pi r^2} = 2A\gamma_{sv} + \gamma_{sv} \left\{ 4^{1/3} \left[\left(\frac{1-A}{1+A} \right)^{1/2} \left(\frac{4+2A}{1+A} \right) \right]^{2/3} - \frac{4}{1+A} \right\} \tag{33a}$$

$$\frac{\Delta G_{syst}}{\pi r^2 \gamma_{sv}} = 2A + 4^{1/3} \left[\left(\frac{1-A}{1+A} \right)^{1/2} \left(\frac{4+2A}{1+A} \right) \right]^{2/3} - \frac{4}{1+A} \tag{33b}$$

A plot of the net integral normalized free energy change vs cos $\phi/2$, which is equal to A in (33b), is shown in Fig. 5. The graph also shows the integral free energy changes due to the solid/solid and solid/vapor area changes. Since solid/solid area is always created by movement of the grain boundary, this factor always makes a positive contribution to the free energy of the system. On the other hand, the solid/vapor area is always reduced and makes a negative contribution; the small contribution at small values of cos $\phi/2$ is a reflection of the small area change because the lenticular pores, with a large dihedral angle, are almost spherical. The net free energy change for the system, however, is always positive throughout the entire range of dihedral angles from 180° to 0° (cos $\phi/2$ = 0 to 1.0).

An effort has not been made here to analyze cases of elongated pores on two or three grain junctions and pores at four grain junctions. Observations have been reported, however, that three grain junctions do not break away from pores.[5,6] Also, it can be deduced by inspection that the breaking away of the grain boundaries from the pore would be energetically even less favorable because the increase of the solid/solid area relative to the decrease in the solid/vapor area would be much larger. From an energetic viewpoint it would be expected that the geometry would change progressively by grain boundary motions to the configuration treated here.

This thermodynamic analysis indicates that the presence of a lenticular pore with any dihedral angle on a planar grain boundary will always pin the grain boundary or the pore will move with the boundary. Thus, for grain boundary movement away from a pore to occur, there must be another negative contribution to the free energy of the system.

B. Lenticular Pore at a Curved Grain Boundary

The geometry to be examined in detail is shown in Fig. 6 which represents a circular sector of width m, arc length L, and angle in terms of Ψ. Then, for a pore-free sector of boundary $L_f = \rho_f\Psi$, the area is $L_f m$ or $\rho_f\Psi m$ and the free energy is $G = \rho_f\Psi m\gamma_{ss}$. A differential change in ρ_f with a constant Ψ leads to

$$dG = \Psi m\gamma_{ss} d\rho_f \tag{34}$$

If $d\rho_f$ is positive, so is dG and vice versa. Therefore, a grain boundary will always have a tendency to move toward its center of curvature with a

constant curvature of Ψ because the incremental free energy change is then negative. Likewise, a movement toward the center of curvature will tend to occur even with a constant chord length if the curvature is decreased in movement because the length of the boundary will then decrease.

The next step is to analyze the free energy changes when a boundary with a pore (L_i) moves to position L_f leaving the pore behind with the geometry of Fig. 6. The sum of the free energy changes due to the creation of the grain boundary and the change in the shape of the pore is positive for all dihedral angles as has been shown in the previous section. There is, however, an additional effect due to the reduction in grain boundary area as the boundary moves toward its center which is always negative. For grain growth or boundary movement to occur, the latter term must have a large enough negative value to make the net free energy change for the system negative. A detailed analysis for movement with constant curvature and within a given sector follows.

The initial area of the grain boundary, making m equal to 2r and neglecting the slight curvature of the boundary through the pore region, is

$$A_{ss}^{I} = L_i(2r) - \pi r^2 = \rho_i \Psi 2r - \pi r^2 \qquad (35)$$

and the final solid/solid interfacial area after movement, where q is equal to the radius of the resulting spherical pore with volume equal to the original lenticular pore, is

$$A_{ss}^{II} = L_f(2r) = \rho_f \Psi 2r = (\rho_i - q)\Psi 2r \tag{36}$$

The change in area is

$$\Delta A_{ss} = 2r\Psi\rho_i - 2r\Psi q - \rho_i \Psi 2r + \pi r^2 \tag{37a}$$

$$\Delta A_{ss} = \pi r^2 - 2r\Psi q \tag{37b}$$

Substituting (17a) into (27) and solving, we get

$$q = \frac{r}{4^{1/3}} \left\{ \left(\frac{1-A}{1+A}\right)^{1/2} \left(\frac{4+2A}{1-A}\right) \right\}^{1/3} \tag{38}$$

Then substituting (38) into (37b) results in

$$\Delta A_{ss} = \pi r^2 - 2\Psi r \left[\frac{r}{4^{1/3}} \left\{ \left(\frac{1-A}{1+A}\right)^{1/2} \left(\frac{4+2A}{1+A}\right) \right\} \right]^{1/3} \tag{39a}$$

$$\Delta A_{ss} = r^2 \left[\pi - \frac{2\Psi}{4^{1/3}} \left\{ \left(\frac{1-A}{1+A}\right)^{1/2} \left(\frac{4+2A}{1+A}\right) \right\}^{1/3} \right] \tag{39b}$$

The change in solid/vapor interfacial area obtained from the planar grain boundary by substituting (17) into (30) is

$$\Delta A_{sv} = \left[4^{1/3} \left\{ \left(\frac{1-A}{1+A}\right)^{1/2} \left(\frac{4+2A}{1+A}\right) \right\}^{2/3} - \frac{4}{1+A} \right] \pi r^2 \tag{40}$$

The free energy change of the system, substituting $\gamma_{sv}2A$ for γ_{ss}, then becomes

$$\Delta G_{syst} = \gamma_{sv}(2A\ \Delta A_{ss} + \Delta A_{sv}) \tag{41}$$

On substituting (39b) and (40) into (41) and solving, we obtain

$$\frac{\Delta G_{syst}}{\pi r^2 \gamma_{sv}} = 2A \left\{ 1 - \frac{2\Psi}{4^{1/3}\pi} \left[\left(\frac{1-A}{1+A} \right)^{1/2} \left(\frac{4+2A}{1+A} \right) \right]^{1/3} \right\}$$

$$+ 4^{1/3} \left[\left(\frac{1-A}{1+A} \right)^{1/2} \left(\frac{4+2A}{1+A} \right) \right]^{2/3} - \frac{4}{1+A} \tag{42}$$

This equation gives the normalized free energy change as a function of angle of curvature (Ψ) for various dihedral angles (represented by A). Solutions for dihedral angles from 168.4° to 106° are plotted in Fig. 7 and for angles from 73.6° to 16.2° in Fig. 8. The integrated free energy curves are positive for low angles of curvature Ψ, and become negative as the angle of curvature increases due to the continuing reduction of the grain boundary length as the curvature becomes larger. Inspection of the graphs indicates that for dihedral angles (ϕ) above about 73° boundary movement can occur at boundary curvatures above about 0.62 radians or about 36°. With the decrease of dihedral angles below 73° boundary movement can occur at decreasing values of curvature; with ϕ at 16°, grain growth can occur at curvatures above about 26°.

Another informative relationship is indicated in Fig. 9 which is a plot of Ψ versus half the dihedral angle $\phi/2$. The locus of points which fall below the curve yield positive values of the free energy for pore isolation, ΔG_{syst}. Whereas, points lying above the curve yield negative ΔG's. Inspection of the graph reveals that the critical angle of curvature is relatively independent of the dihedral angle for large values of $\phi/2$. While at $\phi/2$ less than about 36°, the value of Ψ critical decreases sharply as $\phi/2$ decreases. This result indicates that control of the curvature of the grain boundary is the critical factor in preventing pore isolation and that the introduction of additives to a system causing the γ_{ss}/γ_{sv} ratio to be reduced beyond the critical value has little effect on pinning grain boundaries.

C. Effect of a Mixture of Particle Sizes

A planar cross-section of a model microstructure of an isotropic material with uniform grain size would show hexagonal grains with three grain junctions of 120° and straight line boundaries; the system would then be in metastable equilibrium since there would be no driving force for boundary movement. A variation in grain size would result in grain boundary curvatures because the three grain junctions will always attempt to maintain equilibrium angles of 120°. Grains with less than six sides would have their boundaries curve outward since the polygon angles with straight sides would be less than 120° while grains with more than six sides would have boundaries curving inward since the polygon angles would be greater than 120°. Thus, thermodynamically there would be an additional driving force for a grain with less than six sides to shrink and with more than six sides to grow since the grain boundaries would

have a tendency to move toward their centers of curvature as described above.

With grains of two sizes the length and number of grain boundaries relative to the large grain will be dependent on the size of the small grain. The curvature between the triple points in all cases according to geometry would be spherical and the angle of curvature Ψ would be 60°; therefore, the boundaries would not be pinned by pores. The greater the length of the grain boundary, however, particularly on an atomistic scale, the greater will be the probability that the intermediate portion of the boundary will acquire a smaller angle of curvature because of the driving force to flatten out the boundary. If the curvature decreases below about 36° the pore can then pin the grain boundary. It thus appears that from a thermodynamic viewpoint a starting powder with a single particle size or the smallest particle size range possible is desirable for sintering; the actual size of the particles becomes important only from a kinetic viewpoint.

Conclusions

The thermodynamic analysis of solid state sintering indicates that a decrease in the γ_{ss}/γ_{sv} ratio and an increase in the density of the unfired compact favor densification. An increase in density of the compact results in a greater coordination number for the particles which allows complete densification to be achieved at a higher γ_{ss}/γ_{sv} ratio. This ratio must be less than 1.78 for face-centered cubic packing of uniform spherical particles, 1.59 for body-centered cubic, and 1.31 for simple cubic; correspondingly the dihedral angle has to be larger than 53°, 74°, and 98°, respectively. Therefore, any additives that

would tend to reduce γ_{ss} relative to γ_{sv} would enhance sintering or make sintering possible if the γ_{ss}/γ_{sv} ratio for a given material is above the critical value.

A pore on a planar grain boundary effectively pins the boundary for all values of the γ_{ss}/γ_{sv} ratio and thus the dihedral angle. A curved grain boundary, however, can move away from a pore if the curvature is above the critical value. As the dihedral angle increases above about 73°, although the magnitude of the driving force decreases movement in all cases will occur toward the center of curvature at curvatures above about 36°; as the dihedral angle decreases from 73° to about 16°, the critical curvature value decreases to about 26°. Grain boundaries with lesser curvature tend to be pinned by pores. Additives which reduce the γ_{ss}/γ_{sv} ratio beyond that necessary for dense sintering, therefore, have essentially no effect on the pinning of a grain boundary by a pore.

It thus is evident that the most critical factor in the pinning of grain boundaries by pores is the degree of curvature of the boundaries and not the magnitude of the dihedral angle. Factors that lead to curvature should be controlled. A uniform packing of spheres of a given size should density to a microstructure with uniform grain size with planar grain boundaries. Compacts with a range of particle sizes, however, will tend to form curved grain boundaries. If this curvature is above about 35°, the boundaries will be able to move away from pores. Narrow particle size ranges will tend to form grain boundaries with smaller curvatures.

Another factor that has not been discussed or analyzed is the effect of anisotropy of interfacial energies. Irregular movement of grain

0 0 0 0 3 9 0 2 0 0 3

boundaries and different angles at three grain junctions due to anisotropy could lead to boundary curvatures that would allow them to break away from pores. Additives in this case could be beneficial if their effect would be to reduce any existing anisotropy.

All of the discussions have been based on a uniform and homogeneous distribution of particles. Poor processing that would introduce varying packing densities or introduce agglomerates of higher or lower density than the matrix would result in a range of grain sizes in the early stages of sintering as well as introduce other factors that would interfere with realizing theoretical density in the entire compact. An additive in this case would have a beneficial effect if it played some role in reducing agglomeration or increasing uniformity of particle distribution during the preparation of the compacts.

The presence of a liquid phase at sintering temperatures introduces a degree of complexity in that γ_{ss}, γ_{sv}, $\gamma_{s\ell}$ and $\gamma_{\ell v}$ now play a role in the densification process. A thermodynamic analysis of such systems is being undertaken and will be presented elsewhere.

References

1. I. M. Stephenson and J. White, "Factors Controlling Microstructure and Grain Growth in Two Phase (One Solid + One Liquid) and in Three Phase (Two Solid + One Liquid) Systems," Trans. of British Ceramic Society, Vol. 66 No. 9, 1967.
2. L. Siegle, "Role of Grain Boundaries in Sintering," in Kinetics of High Temperature Processes. Ed. Kingery, W. D., MIT Press, 1959.
3. P. J. Jorgensen, "Modification of Sintering Kinetics by Solute Segregation in Alumina," J. Am. Ceram. Soc., 48, 4, 1965.
4. J. Burke, "Role of Grain Boundaries in Sintering," J. Am. Ceram. Soc., 40, 3, 1957.
5. W. D. Kingery and B. Francois, "Grain Growth in Porous Compacts," J. Am. Ceram. Soc., 48, 10,
6. A. Mocellin and A. Accary, "Study on the Size and Location of Pores During Grain Growth in Hydrogen Sintered Alumina," in Material Science Research - Sintering and Related Phenomena, Vol. 6, Ed. Kuczynski, Plenum Press, 1973.

Figure Captions

Fig. 1. (a) Idealized model of uniform sized spherical particles in simple cubic packing; (b) Two sphere densification model.

Fig. 2. Critical surface energy ratios for densification to theoretical density in solid phase sintering at different packing densities.

Fig. 3. Integral normalized free energy change at the critical surface energy ratio for simple cubic packing.

Fig. 4. Lenticular pore at a planar grain boundary before and after the grain boundary sweeps past.

Fig. 5. Integral normalized free energy change versus dihedral angle for isolation of a lenticular pore at a planar grain boundary.

Fig. 6. A lenticular pore at a curved grain boundary with a constant angle of curvature.

Fig. 7. Normalized integral free energy change for isolation of a lenticular pore at a curved grain boundary versus angle of curvature, at high dihedral angles.

Fig. 8. Normalized integral free energy change for isolation of a lenticular pore at a curved grain boundary versus angle of curvature, at low dihedral angles.

Fig. 9. Critical angle of curvature for pore isolation versus dihedral angle.

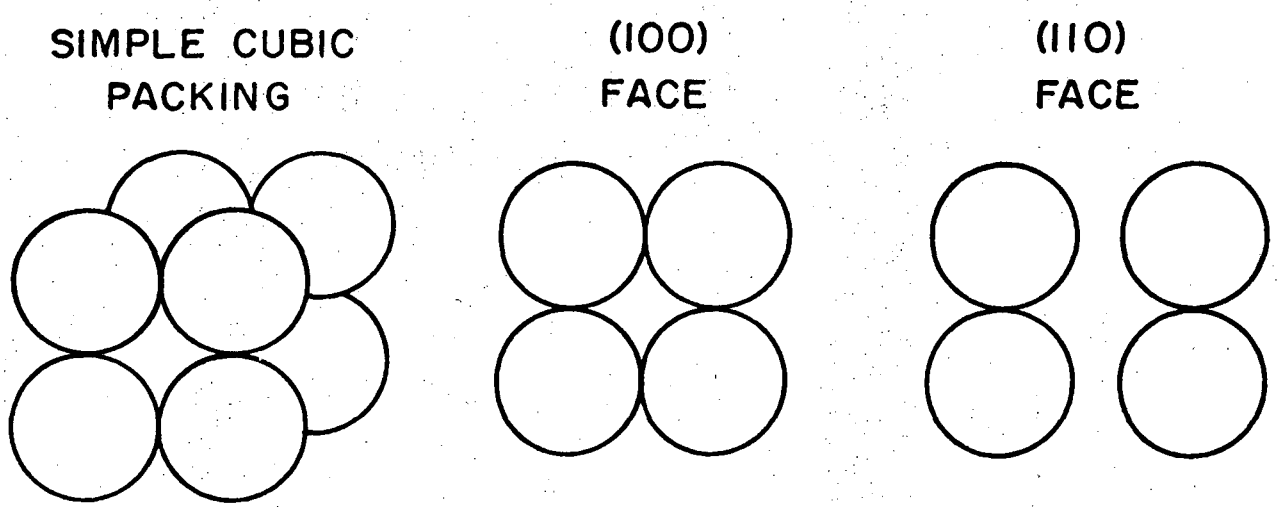

CIRCULAR CAP OF HEIGHT h REMOVED
DURING SINTERING

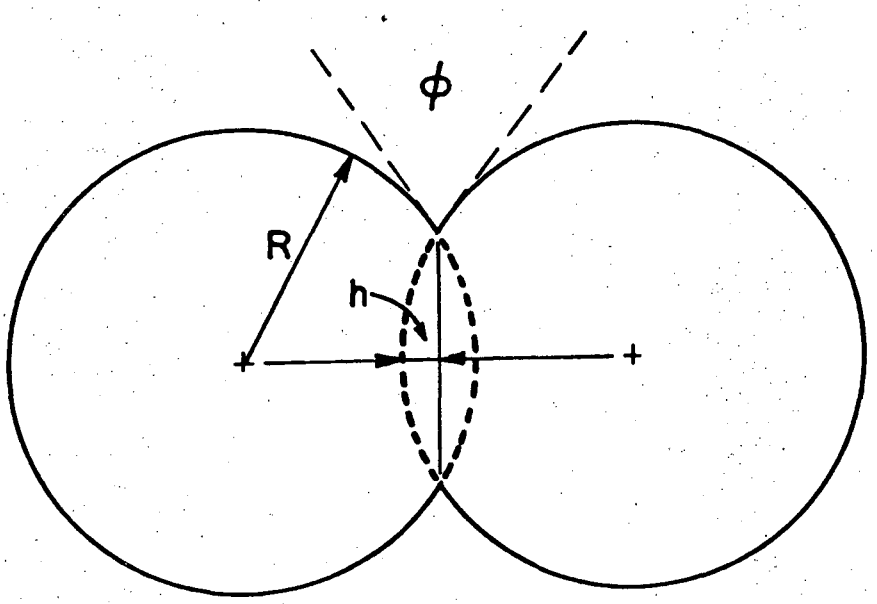

XBL 733-5900

Fig. 1

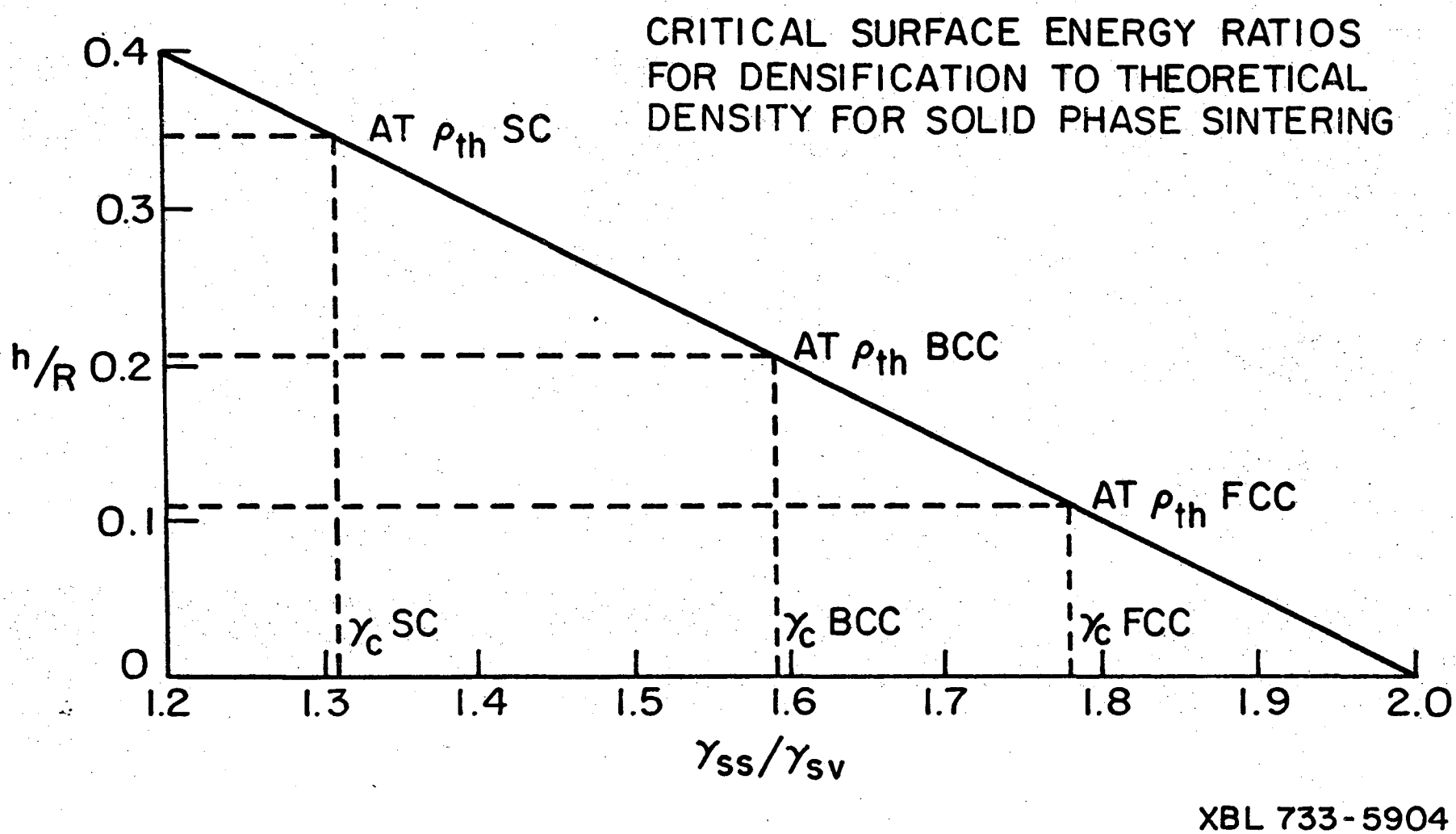
CRITICAL SURFACE ENERGY RATIOS
FOR DENSIFICATION TO THEORETICAL
DENSITY FOR SOLID PHASE SINTERING
0.4
0.3
h/R 0.2
0.1
0
AT ρth SC
AT ρth BCC
AT ρth FCC
γc SC
γc BCC
γc FCC
1.2
1.3
1.4
1.5
1.6
1.7
1.8
1.9
2.0
γss/γsv
XBL 733-5904

Fig. 2

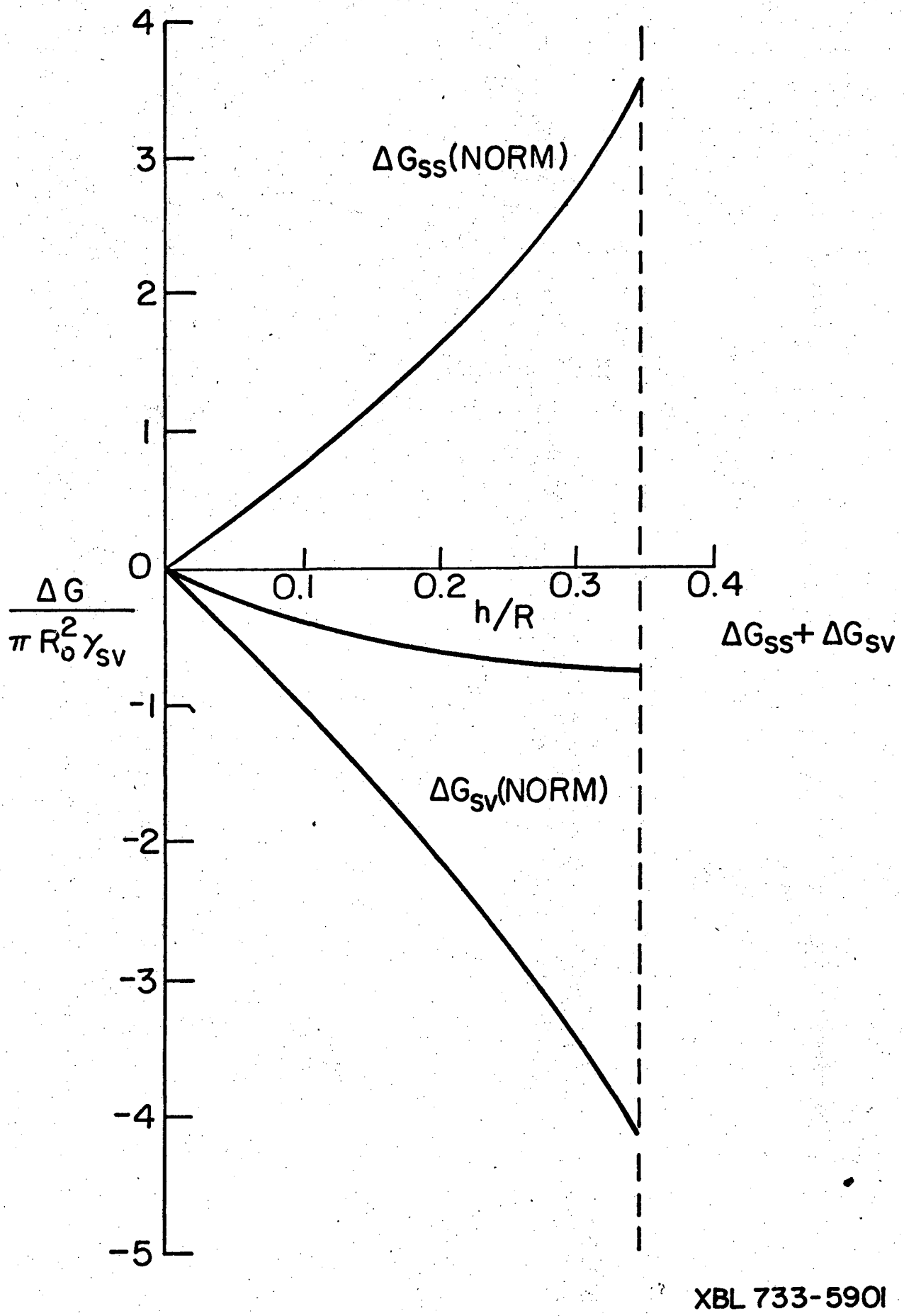
4
3
2
1
0
-1
-2
-3
-4
-5
0.1
0.2
0.3
0.4
h/R
$\frac{\Delta G}{\pi R_o^2 \gamma_{sv}}$
ΔG_{ss}(NORM)
$\Delta G_{ss} + \Delta G_{sv}$
ΔG_{sv}(NORM)
XBL 733-5901

Fig. 3

0 0 0 0 3 6 9 1 2 5 8 6

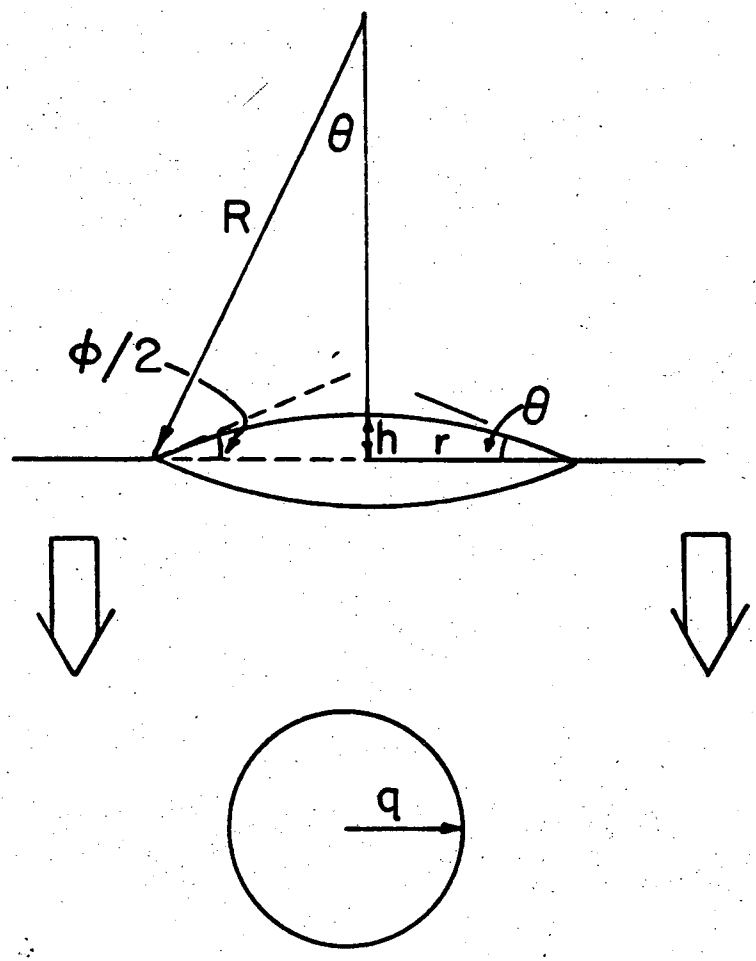

VIEW PERPENDICULAR TO THE PLANE OF THE GRAIN BOUNDARY

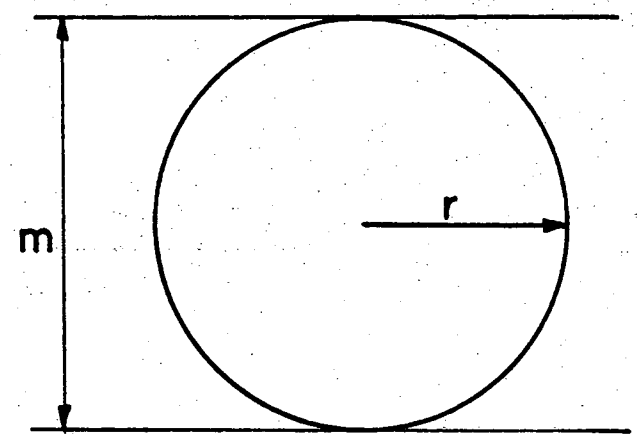

VIEW IN PLANE OF THE GRAIN BOUNDARY

XBL 733-5896

Fig. 4

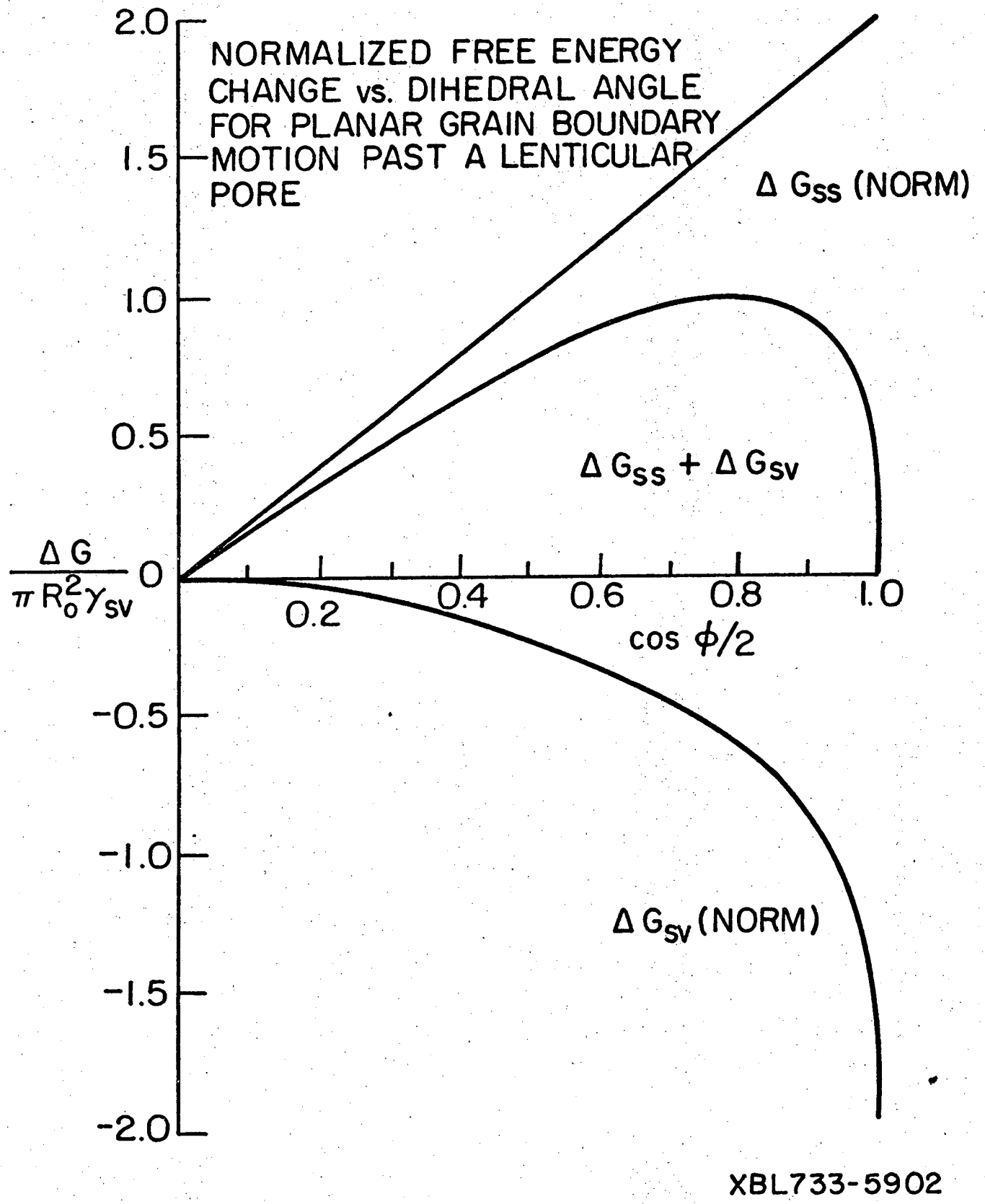

XBL733-5902

Fig. 5

0 0 0 0 3 9 0 2 0 8 7

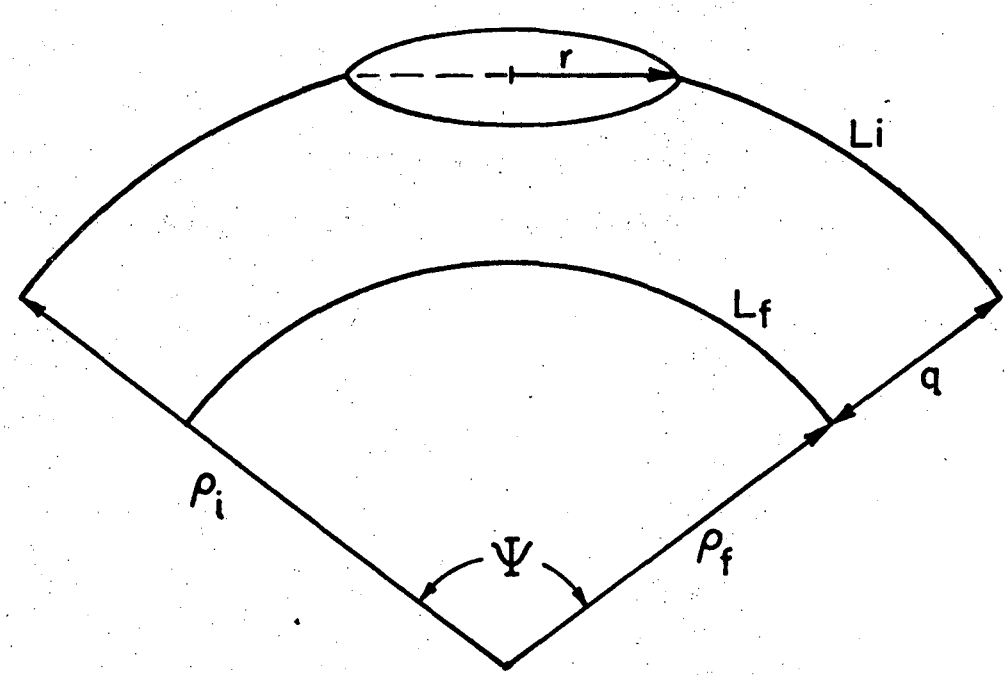

LENTICULAR PORE
AT A CURVED GRAIN BOUNDARY

XBL 733-5899

Fig. 6

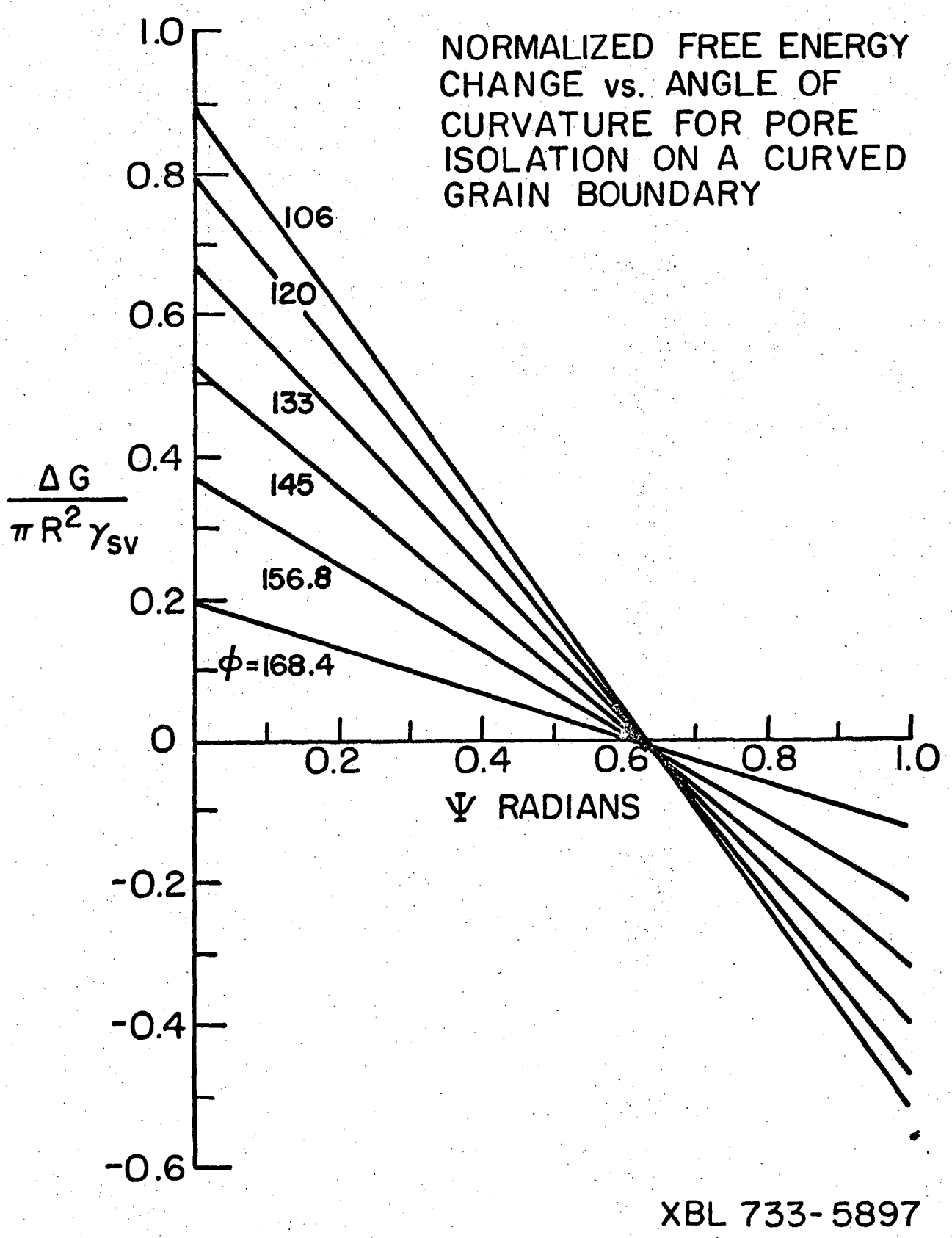
NORMALIZED FREE ENERGY CHANGE vs. ANGLE OF CURVATURE FOR PORE ISOLATION ON A CURVED GRAIN BOUNDARY
1.0
0.8
0.6
0.4
0.2
0
-0.2
-0.4
-0.6
$\frac{\Delta G}{\pi R^2 \gamma_{SV}}$
106
120
133
145
156.8
ϕ=168.4
0.2
0.4
0.6
0.8
1.0
Ψ RADIANS
XBL 733-5897

Fig. 7

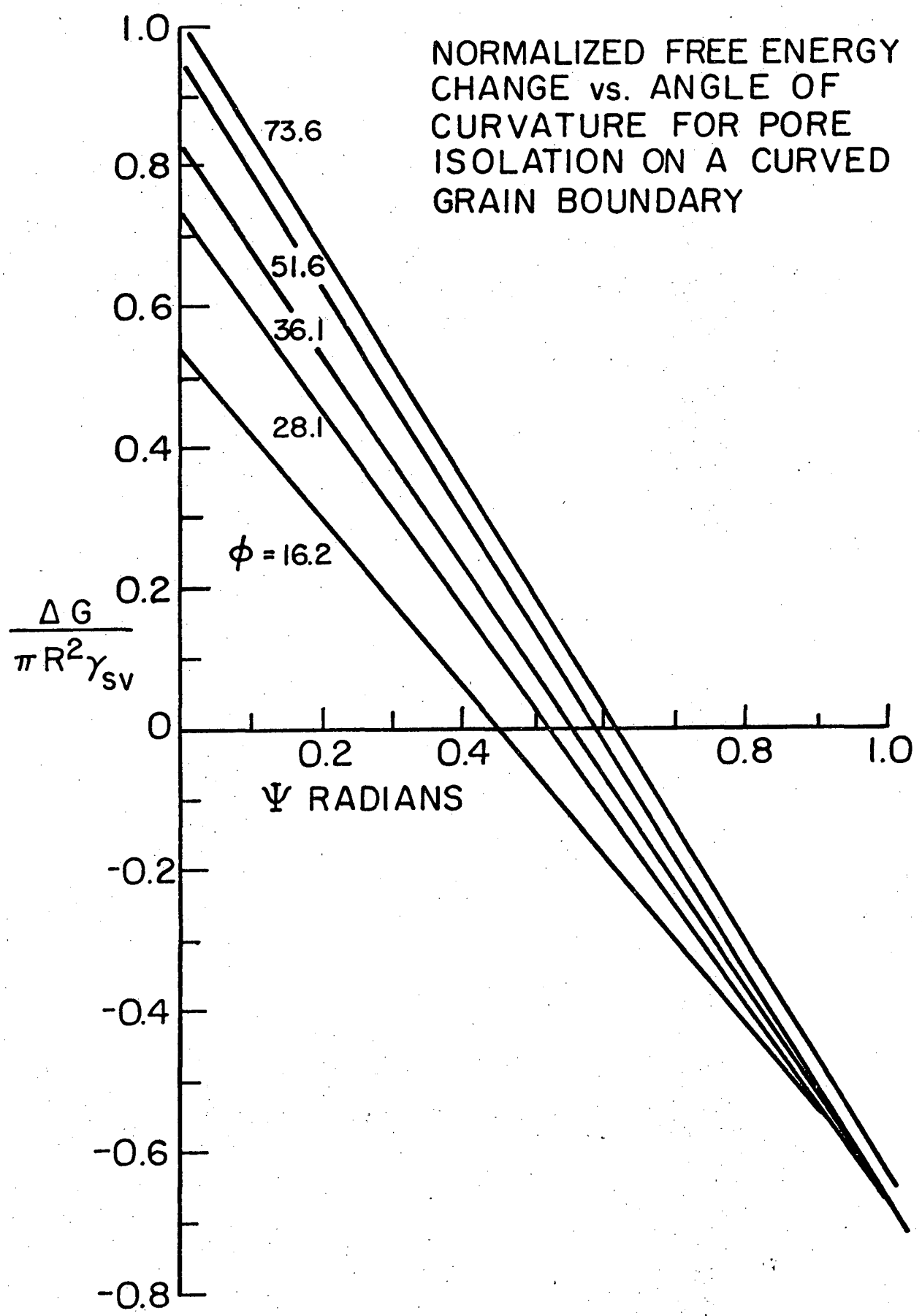

XBL 733-5898

Fig. 8

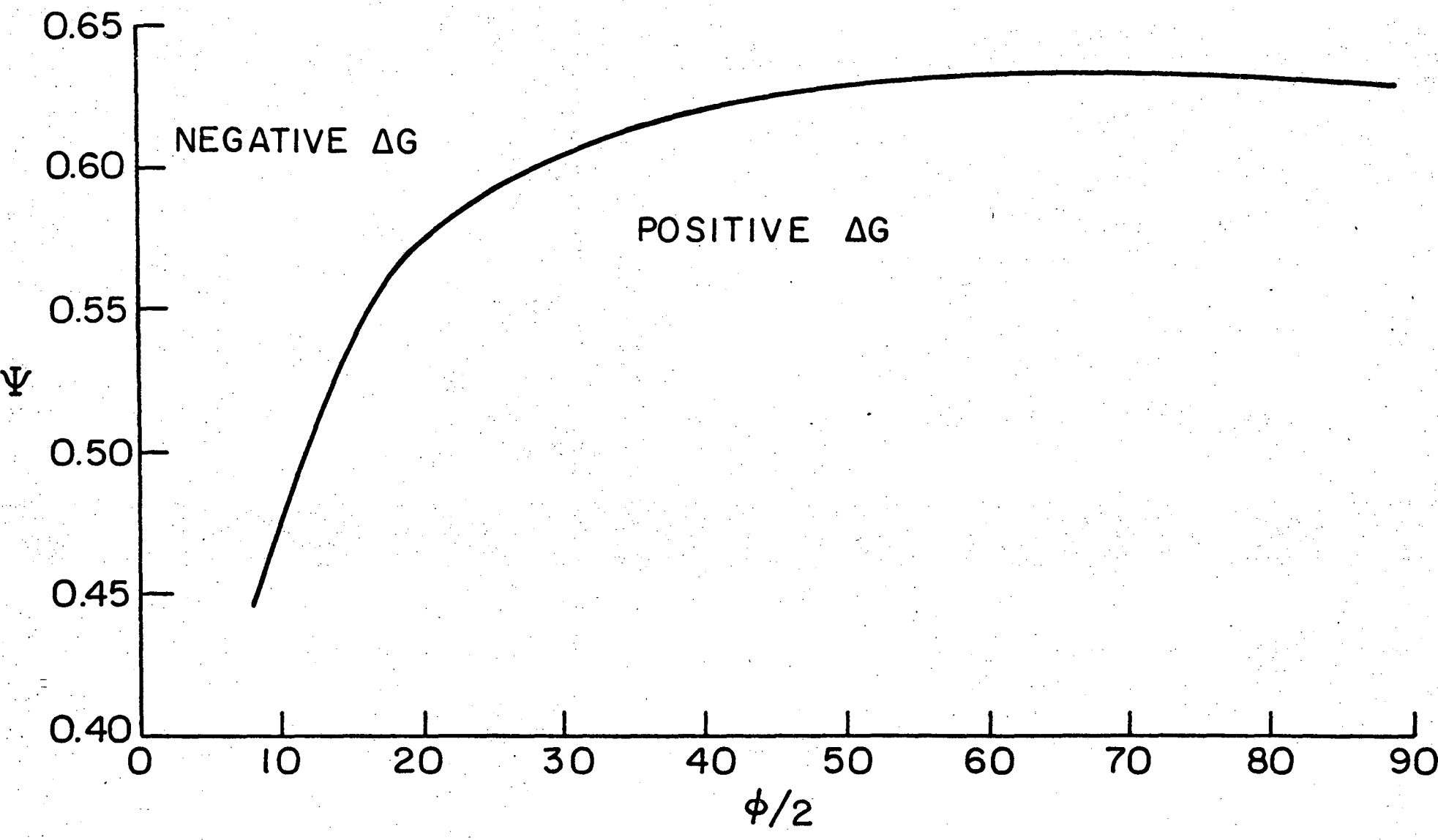

Fig. 9

XBL 733-5903

LEGAL NOTICE

This report was prepared as an account of work sponsored by the United States Government. Neither the United States nor the United States Atomic Energy Commission, nor any of their employees, nor any of their contractors, subcontractors, or their employees, makes any warranty, express or implied, or assumes any legal liability or responsibility for the accuracy, completeness or usefulness of any information, apparatus, product or process disclosed, or represents that its use would not infringe privately owned rights.

TECHNICAL INFORMATION DIVISION
LAWRENCE BERKELEY LABORATORY
UNIVERSITY OF CALIFORNIA
BERKELEY, CALIFORNIA 94720